Journal of Controlled Release 305 (2019) 101–109

Contents lists available at ScienceDirect

Journal of Controlled Release

journal homepage: www.elsevier.com/locate/jconrel

Characterization of jet injection efficiency with mouse cadavers

Jeremy O. Marston*, Carla M.R. Lacerda

Department of Chemical Engineering, Texas Tech University, Lubbock, TX 79409, United States of America

ARTICLE INFO

Keywords:
Mouse cadaver
Needle-free injection
Liquid jet
Intradermal
Intramuscular

ABSTRACT

Needle-free drug delivery is highly sought after for reduction in sharps waste, prevention of needle-stick injuries, and potential for improved drug dispersion and uptake. Whilst there is a wealth of literature on the array of different delivery methods, jet injection is proposed as the sole candidate for delivery of viscous fluids, which is especially relevant with the advent of DNA-based vaccines. The focus of this study was therefore to assess the role of viscosity and jet configuration (i.e. stand-off relative to the skin) upon injection efficiency for a fixed spring-loaded system (Bioject ID Pen). We performed this assessment in the context of mouse cadavers and found that the dominant factor in determining success rates was the time from euthanasia, which was taken as a proxy for the stiffness of the underlying tissue. For overall injection efficiency, ANOVA tests indicated that stiffness was highly significant ($P < < 0.001$), stand-off was moderately significant ($P < 0.1$), and viscosity was insignificant. In contrast, both viscosity and standoff were found to be significant ($P < 0.01$) when evaluating the percentage delivered intradermally. Using high-resolution micro-computed tomography (μ-CT), we also determined the depth and overall dispersion pattern immediately after injection.

1. Introduction

Routine vaccinations are most commonly administered by hypodermic needle and syringe (HNS) [1–4], which are known to cause patient anxiety for a significant number of people [5,6]. This traditional approach also generates sharps waste and a large number of needle-stick injuries, which can be costly to treat [7–10]. However, it is the advent of both novel nucleic acid vaccines [11–15] and fractional dose vaccination [16–19] that could present the biggest challenge yet for needle-based delivery. This is due to a confluence of potentially high-viscosity of the vaccine (up to $\mu \sim 100$ mPa.s for high-concentrations) and the narrow target area for delivery, which is primarily the intradermal (ID) region of the skin.

ID injection of low-viscosity vaccine by standard hypodermic needle and syringe (HNS) can be achieved with the Mantoux technique, but requires a highly skilled practitioner to insert a needle at a low angle relative to the skin. A successful injection into the ID region of the skin is then characterized by a raised circular area (wheal) which has a blanched appearance [20,21]. In particular, a volume of 0.1 ml delivered into the ID region is expected to leave a skin wheal of approximately 6–10 mm [21].

Even if the Mantoux technique is correctly performed and the needle bevel is in the ID tissue, the key component for novel vaccines that could lead to a failed injection is the high-viscosity [22,23]. This is due to the fact that pressure drop along a needle is proptional to viscosity [24] ($\Delta P \propto \mu l V/d^2$), therefore a substantial and sustained force is needed to dispense the drug from a syringe, making it difficult to hold a HNS in a fixed position.

One candidate that holds the potential to deliver high-viscosity fluids is jet injection, which has a long history in both sub-cutaneous and intramuscular delivery [25,26], and has typically relied upon creating a high upstream pressure, using either a spring or compressed gas mechanism, to force a liquid jet at high-speed, $V_{jet} \sim$ O(100 m/s), from a narrow orifice, $D_0 \sim$ O(100 μm). Studies with both commercial and custom devices in the literature [27–49] have comprised a combination of in-vitro [27–35], ex-vivo [36–45], and in-vivo [46–49] and primarily considered large doses (ml) for SC and IM delivery, although some doses down to the nano-liter range have also been reported [50]. Recently, however, we note that new methods are being explored - such as voice coil actuators [43–45] for either intradermal or intramuscular injection, laser-induced jets [51–54] primarily for intradermal delivery, and explosively-driven jets [55]. As such, jet injection now holds promise for ID delivery of fractional doses (0.1 ml), as documented in recent clinical trials [56–65]. Needle-free devices also alleviate anxiety associated with HNS delivery [5,6], needle-stick injury treatment, and sharps waste in resource-limited environments [1–4], and thus must be pursued.

The injectable drug market covers a range of fluid viscosities [66],

* Corresponding author.
E-mail address: jeremy.marston@ttu.edu (J.O. Marston).

https://doi.org/10.1016/j.jconrel.2019.05.023
Received 11 February 2019; Received in revised form 29 April 2019; Accepted 14 May 2019
Available online 18 May 2019

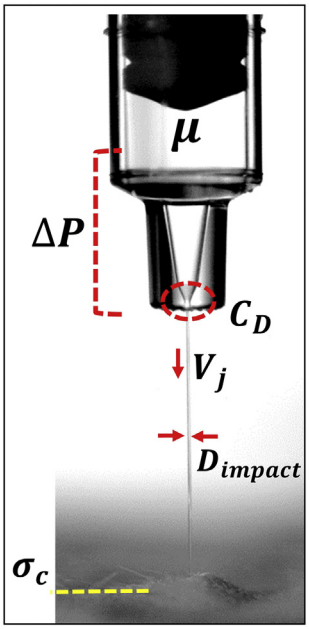

Fig. 1. Overview of fluid mechanical considerations in jet injection, showing total pressure drop, $\Delta P \sim O(10^7)$ Pa, fluid viscosity, μ, orifice discharge coefficient, C_D, jet stream velocity, V_j, actual jet diameter at impact, D_{impact}, and critical stress of the skin, σ_c.

and thus the influence of fluid properties must be considered. For jet injection, with a fixed force or applied pressure (as in our system), fluid mechanical considerations [24], as shown in Fig. 1 (e.g. Hagen-poiseuille law) dictactes that increasing viscosity will reduce flow rate through an orifice, and hence render a reduced jet speed. For jet injector devices, typical pressures generated in the ampoule or cartridge are $O(10^7)$ Pa which, in a purely inertial (inviscid) system using Bernoulli's equation, implies jet speeds of $V_j \approx \sqrt{2\Delta P/\rho} \approx 140$ m/s. However, the frictional head loss through the orifice becomes significant for viscous fluids and the jet speed can be approximated from the energy equation as $V_j \approx \sqrt{2\Delta P/\rho(1 + C_D)}$, where C_D is a discharge coefficient summarizing the viscous loss. Upon exit from the orifice, the jet may travel through air (if a stand-off spacer is used) and then impact skin. Due to the high jet speeds, the jet Weber numbers, $We = \rho D_j V_j^2/\sigma$, are $\sim O(10^4)$ which means the liquid jet will not disintegrate [67]. At the impact stage, the force generated is sufficiently high to overcome the critical stress [42] of the skin, σ_c and puncture into the underlying tissue. However, it must be noted that impact force of the jet is not only a product of jet speed, but also jet collimation (i.e. slender vs. dispersed jet stream), which affects the impact footprint, both of which are affected by fluid viscosity [68]. Furthermore, The interaction of the high-speed jet with the tunderlying tissue, which is heterogeneous and poro-elastic, is a complex fluid-structure phenomena, and has not been properly addressed in the literature. A such the effect of viscosity in this process is not fully understood.

The principal aim of this study was therefore to assess the role of viscosity in jet injection. In particular, does viscosity determine injection depth and overall injection efficiency? *We* performed this assessment in the context of mouse cadavers, in order to facilitate high-resolution micro-computed tomography (μ-CT), but found that the effects of configuration, i.e. stand-off distance of the jet orifice from the skin, and the tissue stiffness are more signifcant. From the (μ-CT) imaging we also determined the depth and overal dispersion pattern immediately after injection. The reader should keep in mind that the use of mice herein was primarily a tool to evaluate the key factors of viscosity, standoff and tissue stiffness, and that for translational research, a more clinically relevant model such as guinea pig would be needed to verify the results.

2. Materials and methods

2.1. Injection device

The jet injector used in this study was the Bioject ID Pen, which is a streamline investigational device originally designed for intradermal injection into human subjects for a variety of drug formulations. The device, shown in Fig. 2(a), comprises a spring housed in an upper chamber which is cocked by manually extending the arm on the outside of the chamber. A cartridge, shown in Fig. 2(b), pre-loaded with fluid is then inserted into the front end of the device and locked in place by rotation. The injection is then triggered manually by pressing on an external trigger ring, whereupon the spring is released and a piston hits the rear end of the plunger. After injection, the used cartridge is released from position by pulling on a release ring.

The cartridges can hold a total volume of 110 μl, and the expelled volume can be set to either 50 or 100 μl (0.05 or 0.1 ml). The upper cartridge inner diameter where the plunger travels is $D_p = 4.57$ mm, whilst the orifice from where the jet exits is circular with a diameter of $D_j = 157$ μm, which was previously reported to provide maximum injection efficiency [39].

In practice, an additional spacer attachement, featured in Fig. 2(b), can be fitted to the end of the cartridge. This serves to implement a stand-off distance, $S = 16$ mm, between the orifice and the skin, and prevent splashing from any rejected fluid (see Fig. 2(c)). For our study, we performed approximately half of the jet injections with the spacer attachment, i.e. $S = 16$ mm, and half with a modified spacer set to zero standoff, i.e. $S = 0$.

2.2. Fluid properties

For this study, Optiprep density gradient medium, procured from Sigma Aldrich, was used as the contrast agent for the CT imaging. In addition, mixtures of Optiprep with both water and glycerin (both at 50%w/w) were used in order to vary the fluid viscosity. The mixtures used herein were chosen to approximate the range of apparent viscosities that could result from the combination of high-shear at the orifice and non-Newtonian nature of many novel nucleic acid vaccines. The fluid properties are are summarised in Table 1, along with the corresponding jet velocities, V_j, and jet powers, $P_j = \frac{\pi}{8}\rho D_j^2 V_j^3$. The jet velocities were calculated using mass conservation from direct measurements of the plunger displacement according to $V_j = (D_P/D_j)^2 V_p$, where $V_P = dZ_P/dt$ is the plunger speed through the cartridge. Across 10 repeat measurements, the jet speed was found to be consistent to within ± 3 m/s in all cases (i.e. within 2%).

The fluids were also dyed with Trypan blue (0.5%w/w) to facilitate visual inspections of any fluid rejection, however this did not result in any noticeable change in fluid density or viscosity.

2.3. Mouse cadavers and injection protocols

For this study, we used mouse cadavers with a time from euthanasia of thirty minutes up to four hours, with the exact time recorded for each animal. The subjects were C57BL/6 J mice procured from Jackson Laboratories used primarily in another in-vivo study, but euthanized at 13 weeks old for purposes of harvesting heart tissues in accordance with institutional guidelines under IACUC protocol 18006-01. As such, the choice of mouse model was dictated primarily by availability. Prior to injection, the mice were weighed and then shaved locally around the thigh/flank region. This injection site was chosen primarily for ease of placement of the spacer due to the location of the underlying thigh muscle. In total, 95 mice (46 males and 49 females) were used in this study with mean body masses of $m = 28 \pm 4$ g and 22 ± 2 g for the males and females resepctively.

A total of 83 jet injections and 13 needle injections were performed into the flank/thigh regions, with a fluid viscosity pre-determined by

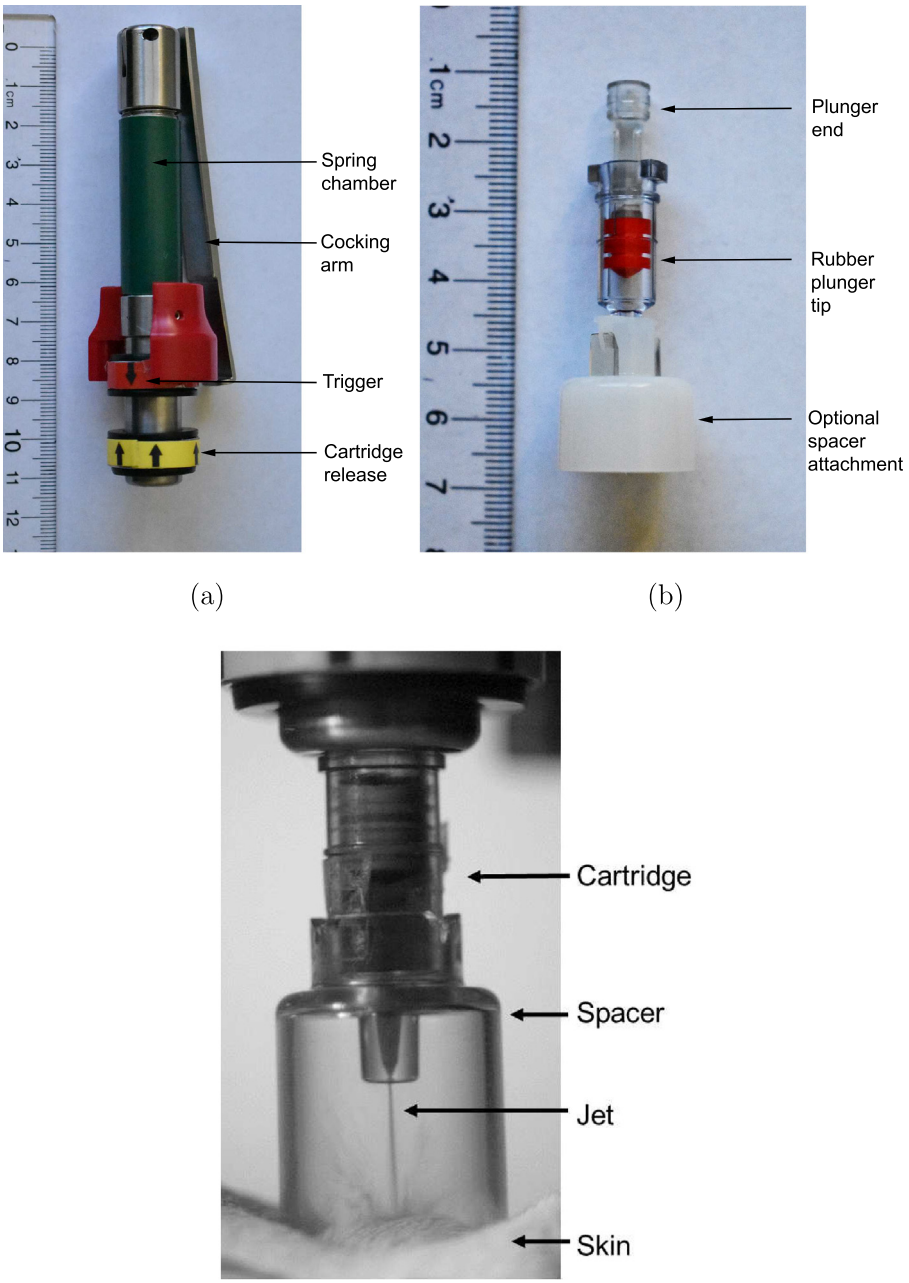

Fig. 2. Photographs of (a) the ID Pen device and (b) standard cartridge for ejecting a volume of 0.1 ml. The white spacer attachment at the end of the cartridge featured in (b) is optional to create a stand-off distance, *S*, of approximately 16 mm. (c) Snapshot from a high-speed video sequence showing implementation of a transparent spacer for visualization purposes.

the experimental design. For the jet injections, the stand-off distance relative to the skin was implemented by use of a spacer, see Fig. 3(a). The complete contact of the spacer to the skin also ensures that the jet is oriented perpendicular to the skin. Minimal applied load was used to avoid bias from both adminstrator, and from animal to animal (due to creep in the underlying tissues). After injection, any rejected fluid remaining on the surface of the skin, see Fig. 3(b), or within the spacer were absorbed by filter paper and weighed on a fine-resolution balance (accuracy ± 0.1 mg). From this mass, m^*, the corresponding injection efficiency could be calculated as

$$E_{\%} = 100 \times \left(1 - \frac{m^*}{\rho V_0}\right) \quad (1)$$

Table 1
Physical properties of the liquids used in the experiments. The mixtures of Optiprep with water and glycerin were approximately 50%w/w.

Liquid	Dynamic viscosity μ (mPa.s)	Density ρ (kg/m^3)	Jet velocity V_j (m/s)	Jet power P_j (W)
Optiprep	11.9	1320	138	33.6
Optiprep + DI water	1.6	1160	152	39.4
Optiprep + glycerin	43.2	1290	136	31.4

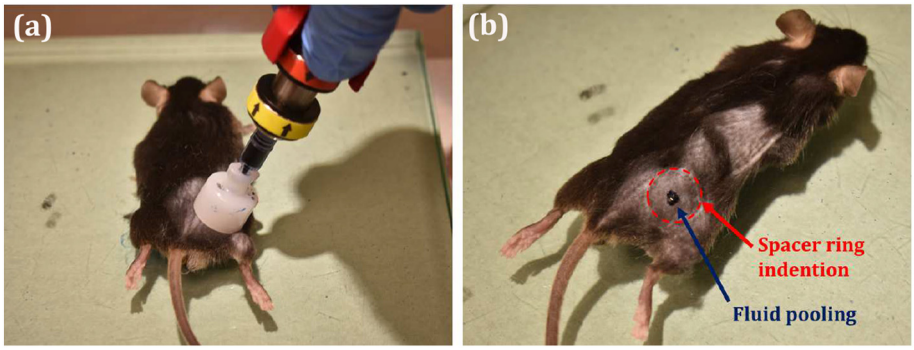

Fig. 3. (a) Orientation of the jet injector with the 16 mm spacer prior to injection, and (b) resulting spacer indention ring and pooling due to fluid rejection.

where $V_0 = 0.1$ ml is the volume expelled from the cartridge in all injections. Whilst the majority of injections were administered via jets, a limited number of supplemental needle-based injections were also performed using the Mantoux technique to the deliver fluid into the ID/SC region. A 30G needle size was used in all cases, which matches the jet diameter, and the delivery volume was also set to 0.1 ml, however, it was not possible to inject the highest viscosity fluid with this technique since the force needed to expel the fluid was so high that the needle tip moved considerably and could not be held in place within the dermal layers.

2.4. Imaging

After injection, the cadaver was placed prone into an IVIS Spectrum CT (Perkin Elmer Inc.) and imaged using the micro-computed tomography (μ-CT) function with a voxel size of 150 µm. The images were then analyzed in Living Image v4.5.5 to render 3D anatomical reconstructions and determine the location of the fluid. The key measurements taken from these images were the depth relative to the injection site and total dispersion pattern. Top-view images were also taken by digital SLR (Nikon D90) to catalog the injection site.

3. Results and discussion

3.1. Qualitative overview: jet vs. needle

Figs. 4–8 present example montages from the μ-CT imaging, showing the different types of injections and outcomes observed in this study. The principal reference case that we use for benchmarking the jet injection is a needle-based Mantoux injection, which is shown in Fig. 4. A 3D rendering of the whole mouse is presented in Fig. 4(a), where the skin has been colored yellow, for visualization purposes, and the fluid deposited under the skin (bleb) is clearly visible in white. The distinct pointed section of this white mound indicates the insertion/retraction site of the needle. By thresholding to eliminate the skin and other tissue, the anatomical structrure is rendered in 4(b) and overlayed with three planar sections, centered through the skin bleb. in particular, the axial (green) and sagittal (blue) planes are presented individually in 4(c) and (d). It is from the axial and sagittal planar sections that we can most readily assess the true dimensions of the injection, such as the maximum lateral extent and depth relative to the skin. In this specific realisation, the bleb has axial and sagittal diameters of 8.7 and 8.4 mm, respectively, whilst the height is approximately 3 mm. (For interpretation of the references to colour in this figure legend, the reader is referred to the web version of this article.)

Fig. 5 presents a corresponding montage of a jet injection performed at zero standoff ($S = 0$), which resulted in the formation of a skin bleb. In this instance, the majority of the injected volume accumulates in the skin, but the jet penetrates deeper into the muscle tissue and deposits a significant volume several millimeters below the original skin surface. From the axial and sagittal views of the bleb, we estimate the diameters to be approximately 7.3 and 7.1 mm, respectively, whilst the height is 2.2 mm. A side-by-side comparison of the skin blebs formed by the needle and jet injections from Figs. 4 and 5 is presented in Fig. 6. The bleb for the jet injection is smaller than for the needle injection as some of the fluid is delivered deeper into the IM region, evidenced by the presence of contrast agent deeper in the muscle tissue in Fig. 6(b); The fact that the intradermal bleb is smaller than for needle injection would be undesirable if ID delivery only is required, however, the required deposition depth and ratio of ID:IM volume may depend upon the nature of the injectant.

Given the symmetrical dome shape, we can estimate the volume remaining in the ID region using a spherical cap approximation, $V = \frac{\pi h}{24}(3d^2 + 4h^2)$, which given $d = 7.3$ mm and $h = 2.2$ mm yields an approximate volume of $V \approx 0.052$ ml, i.e. approximately half of the injected volume. For the needle-based injection, this approximation

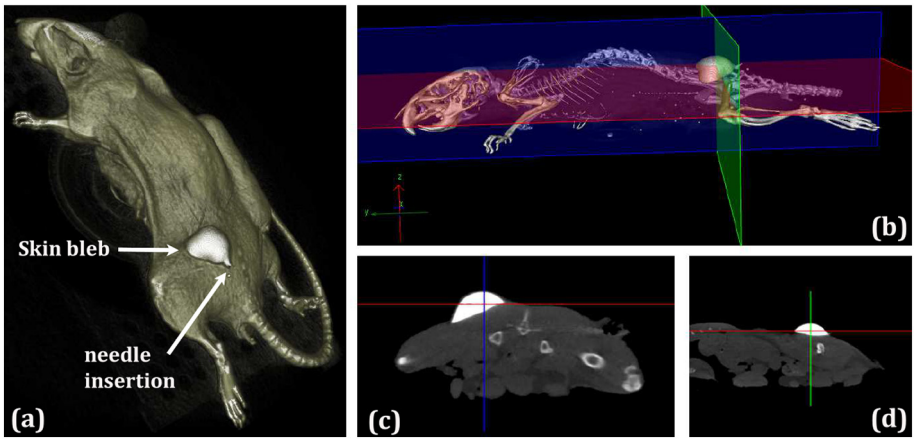

Fig. 4. (a) Micro-computed tomography (μ-CT) image of a mouse cadaver with a single needle injection site on the left flank region. The injection of 0.1 ml Optiprep (contrast agent) was performed with a 30G needle into the ID/SC region. The anatomy in (b) indicates the three planar sections centered across the injection site, with the axial and sagittal planes shown in (c) and (d).

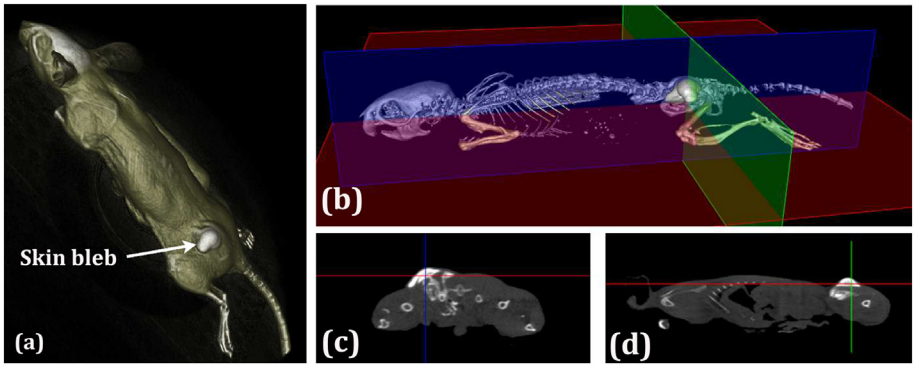

Fig. 5. (a) Micro-computed tomography (μ-CT) image of a mouse cadaver with a single jet injection site on the left flank region. The jet injection of 0.1 ml Optiprep (contrast agent) was performed at $S = 0$. The anatomy in (b) indicates the three planar sections centered across the injection site, with the axial and sagittal planes shown in (c) and (d). Approximately half of the injected fluid remains in the intradermal and sub-cutaneous tissue.

yields 0.097 ml, which is in very good agreement with the total injection of 0.1 ml, indicating that this method provides a sound estimate of volume remaining in the ID region.

In many cases, we observed this combination of both ID and IM delivery with varying volumes deposited into the respective tissues. An example whereby the majority of the injected volume is delivered into the IM tissue is presented in Fig. 7. Here, we observed a small skin bleb around the injection site, but a large volume dispersed laterally in the thigh muscle underneath the femur. The 3D anatomical reconstructions, shown in Fig. 7(b) and (c), are particularly descriptive as they reveal the jet path in front of the femur down to the thigh muscle, and the final dispersion pattern, which appears to be an elongated thin pool, rather than a circular 'bolus' formation. In this case, the maximum depth reached was 6.2 mm and the laterally dispersion (seen in Fig. 7(b) and (c)) is approximately 15.5 × 6.1 mm.

Lastly, we present in Fig. 8 an example of a failed injection, in which the jet completely punctures the mouse and deposits most of the delivered volume into the abdomen of the mouse. The fluid accumulation is seen in the CT image in 8(b), whilst the true jet path can be seen from the axial plane in (c). As discussed below in Section 3.2 the outcome (success vs. fail) depends upon several factors, but primarily is due to stiffness of the cadaver tissue. In a few realizations, we observed complete rejection, however, the typical failed injection was manifested by pierce-through, ie. injections where the jet penetrates completely through the mouse, and does not leave a bleb or IM deposit.

3.2. Success rates and injection efficiency

For an overview of the ensemble data, we present Figs. 9 and 10 that show the overall success rates and injection efficiencies, $E_{\%}$, for the jet injections where, as stated previously, we define a successful jet injection as one which does not puncture the entire cadaver (see Fig. 8), and the efficiency as the ratio of volume delivered divided by the volume expelled from the device, as per Eq. (1).

The overall success rate for all of the jet injections administered in this study was 60%, with the highest success rates observed for the medium viscosity ($\mu = 11.8$ mPa.s), see Fig. 9(a) and the zero stand-off configuration ($S = 0$ mm), see Fig. 9(b), at 68% and 65% respectively. However, there is a key factor at play that success rate alone masks, which is the time lapse, t, from euthanasia to injection. By segregating the data into groups for $t < 90$ min and $t > 90$ min, we observe a dramatic discretization. This is best observed by assessing the injection efficiency, $E_{\%}$, as function of both fluid viscosity and stand-off configuration, as shown in Fig. 10(a) and (b). Note that for $t < 90$ min, we do not have data for the medium viscosity - due to limited availability of the mice, we chose to explore the full viscosity range in the regime of $t > 90$ min.

In Fig. 10(a), for injections performed within 90 min of euthanasia, we observe a significant amount of variation in efficiency; for example, for water, the median is $E_{\%} = 61\%$, but the total range is 23–100% and likewise for the higher viscosity fluid, the median is $E_{\%} = 79\%$, but the total range is 0–93%. These data indicate a high degree of variability in injection when the muscle tissue is still pliable (i.e. prior to rigor mortis). In contrast, by inspecting the injections performed at $t > 90$ minutes, there is a notable increase in median injection efficiency *and* decrease in variability, which is evident from the reduced range (both interquartile and full ranges). In fact, the median efficiency for all cases increases to over 95%.

Similarly, with regards to the stand-off configuration, we observe the same dramatic increase in injection efficiency from $t < 90$ to $t > 90$ minutes. For the injections performed at $t < 90$ minutes, the configuration using the spacer with a stand-off of $S = 16$ mm leads to slightly improved performance with a median of $E_{\%} = 79\%$, compared to $E_{\%} = 59\%$ for $S = 0$. In contrast, when we examine the injections performed at $t > 90$ minutes, both configurations show increased efficiencies of 93 and 97%, respectively for $S = 16$ and $S = 0$. Judging solely from these boxplots, we could tentatively conclude that for pliable muscle tissue, a stand-off of $S = 16$ mm performs better than $S = 0$ mm, whilst for muscle tissue that has begun stiffening under rigor mortis, $S = 0$ performs better. At this point, we do not have a quantitative argument which can explain these conflicting observations, however it is clear that stiffness of the underlying tissue is the dominant factor in determining the success and efficiency of the jet injection. The authors are unaware of any publications which report increased injection efficiency with increasing tissue stiffness.

For statistical purposes, single-factor ANOVA tests reveals that the segregation of results by time from euthanasia (i.e. $t < 90$ vs. $t > 90$) is statistically highly significant (P-value $< < 0.001$). In contrast, the effect of standoff for $t > 90$ is moderately significant (P-value of 0.059) and the effect of of viscosity for the data at $t > 90$ is not signficant (P-value > 0.1).

From a fluid mechanics standpoint, it should be noted that

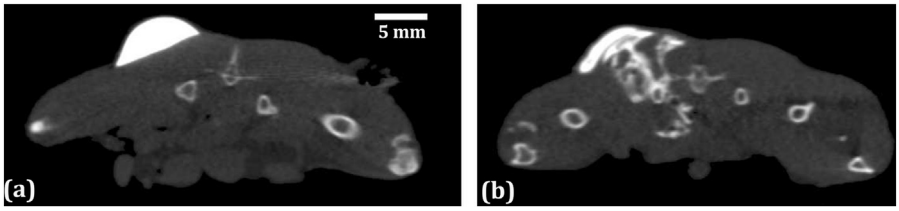

Fig. 6. Comparison of blebs formed via (a) needle and (b) jet injections, for injection volumes of 0.1 ml. The bleb shown in (a) has a diameter of 8.7 mm and height of 3 mm, whilst in (b), the bleb has a diameter of 7.3 mm and height of 2.1 mm.

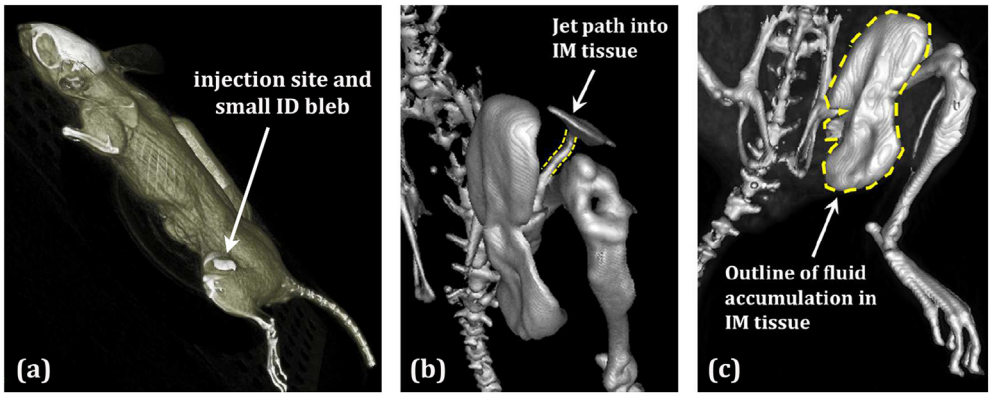

Fig. 7. (a) Micro-computed tomography (μ-CT) image of a mouse cadaver with a single jet injection site on the left flank region. The jet injection of 0.1 ml Optiprep (contrast agent) was performed at $S = 0$. The anatomical reconstructions show (b) the jet path in front of the femur, and (c) overall fluid dispersion into the intramuscular (IM) tissue.

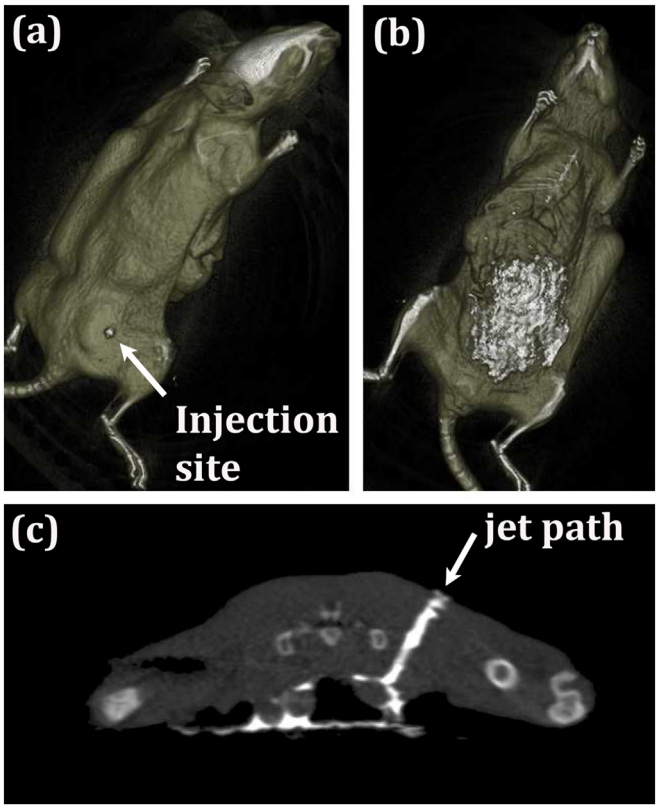

Fig. 8. Micro-computed tomography (μ-CT) images of a failed jet injection showing (a) the injection site on the right thigh, (b) fluid collection on the underside of the mouse, and (c) axial view of the jet path.

increasing viscosity obviously leads to a reduced jet speed [24]. However, the nature of the jet (laminar vs. turbulent) and overall collimation (dispersed vs. slender) of the jet stream may also change [67,68]. Therefore, depending on the stand-off distance, the impact area of the jet can vary, which will affect both the skin puncture and subsequent penetration and dispersion of the jet within the underlying tissues. To fully understand the influence of underlying tissue, further controlled experiments are needed. However, we can qualitatively shed light on the matter in the context of ref. [69], where it was found that soft tissues absorbed more impact energy through deformation. For our case that could lead to dissipation of jet kinetic energy resulting in higher rejection rates. However, it could also manifest by the jet puncturing through the tissue more easily, as exemplified in Fig. 8.

3.3. Intradermal delivery and maximum penetration

To look more closely at the fluid distribution, beyond total volume delivered, we now present in Figs. 11 and 12 data for the percentage delivered intradermally (Fig. 11(a) & (b)), along with the maximum depth and dispersion (Fig. 12(a) & (b)).

In Fig. 11(a) & (b), the percentages are stated as the percentage of the total 0.1 ml ejected by the device, so that 20% ID delivery implies 20 µl remains in the ID region. As such, we observe that for all fluid viscosities, there are trials where there is no intradermal delivery. In such cases, all of the fluid delivered accumulates in the deeper muscle tissue. Furthermore, if we focus on just the lowest and highest viscosity, it is apparent that the cadavers injected at $t < 90$ min exhibit slightly improved performance in terms of ID delivery since up to 25% can remain ID (taking upper quartiles), whereas for $t > 90$ min, these values are less than 10%. From the results at $t < 90$, there is no effect of viscosity. However for $t > 90$, single-factor ANOVA shows that viscosity is significant (using a significance level of 0.01). Upon comparison of just the data for highest and lowest viscosities, we again must conclude that the underlying tissue is the dominant factor. If we take the median percentages as a single quantifier, the data imply that jet injection with the current parameters is not an efficient method for intradermal delivery in mice and that the majority of the injected fluid is deposited into muscle tissue. However, it must also be acknowledged that the device was designed for human delivery and that mice have very thin dermal layers in comparison to other mammals [70]. Replicating the effects observed herein with guinea pigs would be needed for more clinical relevance.

Turning now to the effect of stand-off, in Fig. 11(b), we find that the implementation of a spacer with $S = 16$ mm does provide a superior ID delivery over $S = 0$, whereby the median volume remaining ID is 20 µl compared to less than 10 µl for $S = 0$. Again, single-factor ANOVA tests indicate that the effect of standoff is significant. However, this is only valid for $t < 90$ min, i.e. for pliable underlying tissue. Once rigor mortis has occurred, the effect disappears and both configurations render relatively poor ID delivery with median volumes less than 10 µl.

Finally, we present in Fig. 12(a) & (b) the total penetration depth of the jet and the lateral dispersion, respectively. These measurements are taken at the site of the primary IM deposit occurs. Based on the data in Fig. 11, the IM bolus is nearly always larger than the ID bleb and, again, we find that the dominant factor is the underlying tissue stiffness, deduced by comparing the injections at different times. By inspection of the total ranges, the injections into cadavers for $t > 90$ min appear more consistent, however there is no statistically significant effect of either the time from euthanasia nor the standoff in this case, and all the data is loosely centered around a depth of approximately 8–10 mm for all configurations (viscosities and stand-offs). With reference to Fig. 7, the IM deposit is typically a thin 'pool' or 'puddle'-shape as opposed to a true bolus formation, and Fig. 12(b) plots the lateral extent of these deposits; again, we determine that there is no significant effect in this

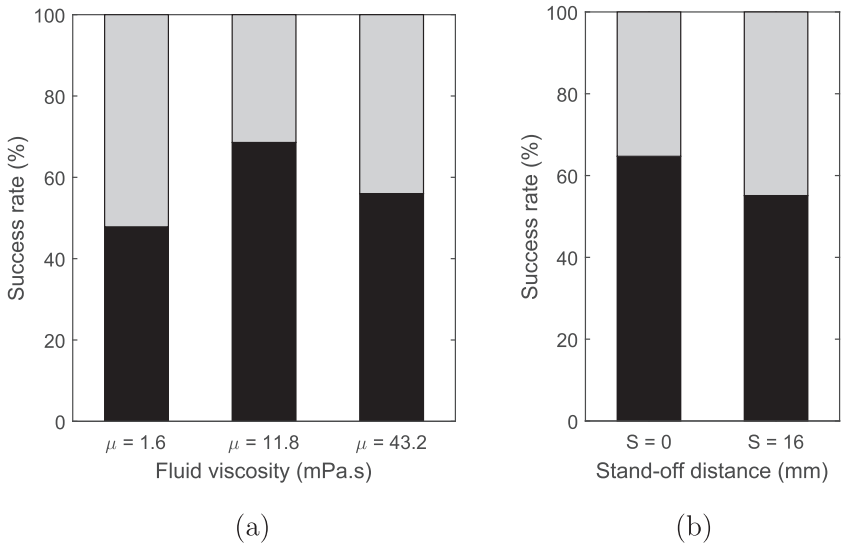

Fig. 9. Success (pass/fail) rates for (a) different viscosities and (b) different stand-offs.

case, and that the lateral extent is typically between 8 and 12 mm, whilst the thickness is on the order of 1–2 mm, which could be an indication of fluid distribution along the orientation of the muscle fibers.

4. Conclusions

In summary, we have conducted a study of jet injection into mouse cadavers, with the aim of elucidating the effect of viscosity and orifice stand-off on injection efficiency and dispersion patterns. The jet orifice diameter used was 157 µm and, with fluid viscosities from 1.6–43.2 mPa.s, the resulting jet velocities ranged from 136 to 152 m/s, which was not only sufficient to penetrate the skin, but deposit fluid into both the intradermal and penetrate to the intramuscular regions. The overall success rate, where fluid was deposited into either the ID/SC/IM regions was 60%, whilst the injection efficiency varied depending primarily on the tissue stiffness. In particular, for cadavers that had undergone rigor mortis (t > 90 min), the majority of injections resulted in a high injection efficiency $E_{\%}$ > 90%, whilst a small number resulted in lower efficiencies. As noted by ref. [38], cadaver skin typically has a lower Young's modulus than living skin, meaning that the jet may penetrate the skin more easily. However, the muscle tissue stiffness increases with time from death, meaning that the properties of both the skin and the underlying tissue likely contribute significantly to the injection process.

Within the subset of successful injections, we noted that of the total ejected volume of 100 µl, less than 25 µl typically remained in the ID region, with the majority of the fluid deposited deeper into the muscle tissue. We acknowledge that the estimate of volume remaining in the ID region is based upon a spherical cap approximation, however, this was shown to be accurate when calibrated against needle-based Mantoux injections.

Whilst the particular jet injector used in this study is not specifically designed for rodents, the data collected herein for the mouse cadavers indicates that the single most important factor determining the outcome of a jet injection is the stiffness of the underlying tissue. Whilst we did not quantify the stiffness of the cadavers, previous measurements [71] for humans in-vivo indicate stiffness is of the order of 100–1000 N/m, which provides a guide to the target range for future work. From our results it is apparent that increasing skin tension or underlying tissue stiffness could increase injection efficiency. Implementing this in a practical manner could be achieved by use of a pre-tensioning device or threshold loading. In light of this, future studies should investigate the role of the applied pressure (of the injector device against the skin), the role of dermal layer thickness, and injection site, using different clinically relevant animal models. Specifically, we hypothesize that increasing applied pressure will increase injection efficiency.

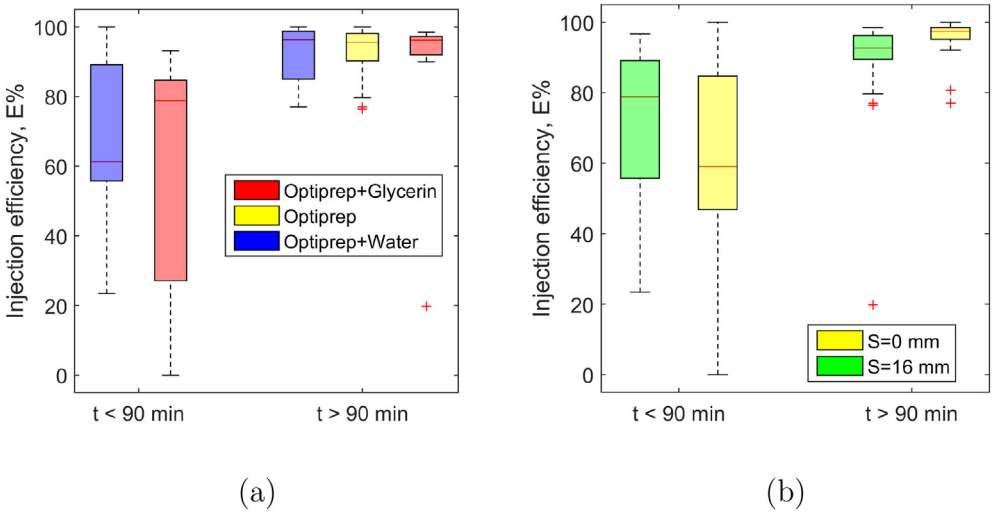

Fig. 10. Injection efficiency for (a) different viscosities and (b) different stand-offs. In both plots, the data has been categorized into times less than or greater than 90 min. The solid red line marks the median, whilst the edges of the boxes are the upper and lower quartiles. Outliers are marked by the red crosses. (For interpretation of the references to colour in this figure legend, the reader is referred to the web version of this article.)

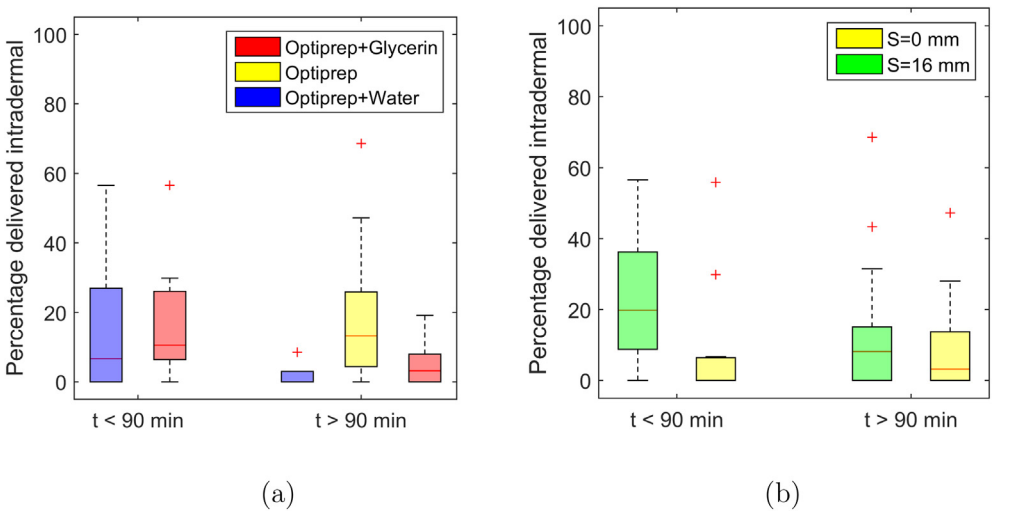

Fig. 11. Percentage of volume deposited intradermally for (a) different viscosities, and (b) different stand-offs, with data categorized into times less than or greater than 90 min. Outliers are marked by the red crosses. (For interpretation of the references to colour in this figure legend, the reader is referred to the web version of this article.)

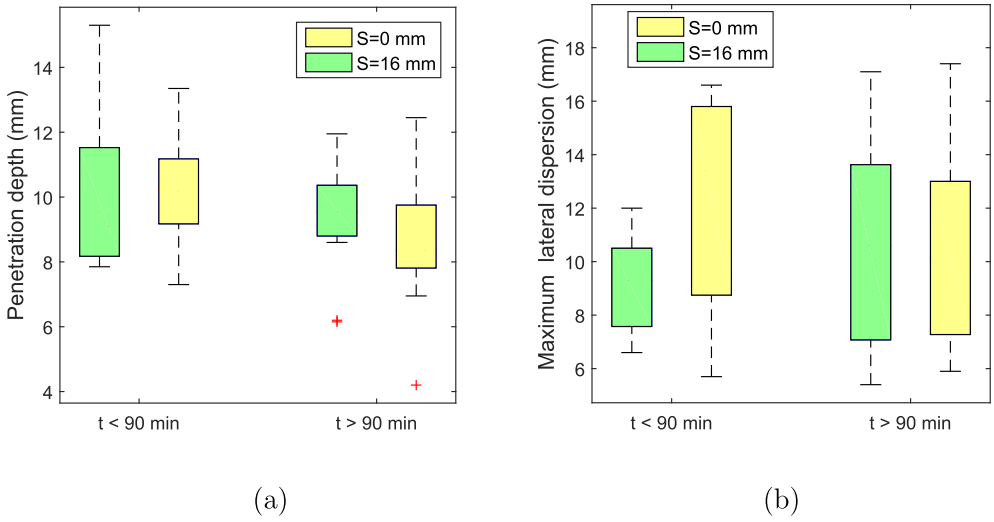

Fig. 12. (a) Penetration depth and (b) Lateral dispersion, with data categorized into times less than or greater than 90 min. Outliers are marked by the red crosses. (For interpretation of the references to colour in this figure legend, the reader is referred to the web version of this article.)

Acknowledgements

This work was financially supported by The National Science Foundation via award number NSF-CBET-1749382. The authors would like to thank the staff of the animal care services and Will Hauser for assistance with the experimental work, and Paul Fisher and Kate Broderick of Inovio Pharmaceuticals for helpful comments on the manuscript preparation. We also thank the anonymous reviewers, whose comments have greatly improved the discussion in this manuscript.

References

[1] L. Jodar, P. Duclos, J.B. Milstein, E. Griffiths, M.T. Aguado, C.J. Clements, Ensuring vaccine safety in immunization programmes - a WHO perspective, Vaccine 19 (2001) 1594–1605.
[2] Proceedings of the Annual Meeting of the Safe Injection Global Network, Dubai 2010.
[3] 2014 Assessment Report of the Global Vaccine Action Plan.
[4] 2016 Secretariat Annual Report of the Global Vaccine Action Plan: Monitoring, Evaluation and Accountability.
[5] Y. Nir, A. Paz, E. Sabo, J. Potasman, Fear of injection in young adults: prevalence and associations, Am. J. Trop. Med. & Hygiene 68 (2004) 341–344.
[6] G.H. Verrips, R.A. Hirasing, M. Fekkes, T. Vogels, S.P. Verloove-Vanhorick, H.A. Delemarre-Van de Waal, Psychological responses to the needle-free MediJector or the multidose Disentronic injection pen in human growth hormone therapy, Acta Paediatr. 87 (1998) 154–158.
[7] A. Kane, J. Lloyd, M. Zaffran, L. Simonsen, M. Kane, Transmission of hepatitis B, hepatitis C and human immunodeficiency viruses through unsafe injections in the developing world: model-based estimates, Bull. WHO 77 (1999) 801–807.
[8] The World Health Report 2002: Reducing Risks, Promoting Healthy Life.
[9] A. Mannocci, G. De Carli, V. Di Bari, R. Saulle, B. Unim, N. Nicolotti, L. Carbonari, V. Puro, G. La Torre, How much do Needlestick injuries cost? A systematic review of the economic evaluations of needlestick and sharps injuries among healthcare personnel, Infect. Control Hosp. Epidemiol. 37 (2016) 635–646.
[10] J. Jagger, E.H. Hunt, R.D. Pearson, Estimated cost of needlestick injuries for six major needled devices, Infect. Control Hosp. Epidemiol. 11 (1990) 584–588.
[11] M.A. Liu, DNA vaccines: a review, J. Intern. Med. 253 (2003) 402–410.
[12] M.A. Kutzler, D.B. Weiner, DNA vaccines: ready for prime time? Nat. Rev. Genet. 9 (2008) 776–788.
[13] J. Rice, C.H. Ottensmeier, F. Stevenson, DNA vaccines: precision tools for activating effective immunity against cancer, Nat. Rev. Cancer 8 (2008) 108–120.
[14] S.S.A.A. Hasson, J.K.Z. Al-Busaidi, T.A. Sallam, The past, current and future trends in DNA vaccine immunizations, Asian Pacific J. Top. Biomed. 5 (2015) 344–353.
[15] J.K. Vasir, V. Labhasetwar, Targeted drug delivery in cancer therapy, Tech. Cancer Res. Treatment 4 (2005) 363–374.
[16] J. Hickling, R. Jones, Intradermal delivery of vaccines: a review of the literature and the potential for development for use in low- and middle-income countries, WHO Report, 2009.
[17] J.-F. Nicolas, B. Guy, Intradermal, epidermal and transcutaneous vaccination: from immunology to clinical practice, Expert Rev. Vaccines 7 (2008) 1201–1214.
[18] P.H. Lambert, P.E. Laurent, Intradermal vaccine delivery: will new delivery systems transform vaccine administration? Vaccine 26 (2008) 3197–3208.
[19] Gupta, J., Park, S., Bondy, B., Felner, E.I. & Prausnitz, M.R., Infusion pressure and pain during microneedle injection into skin of human subjects Biomaterials 32, 6823–6831.

[20] Springhouse, Portable LPN: The all-in-one Reference for Practical Nurses, Lippincott, Williams & Wilkins, Philadelphia, 2005.
[21] Skin testing for tuberculosis, in: C.C. Dasco, Walker, Hall, Hurst (Eds.), Clinical Methods: The History, Physcial and Laboratory Examinations, Butterworths, 1976.
[22] F. Cilurzo, F. Selmin, P. Minghetti, M. Adami, E. Bertoni, S. Lauria, L. Montanari, Injectability evaluation: an open issue, Pharm. Sci. Tech. 12 (2011) 604–609.
[23] A. Allahham, D. Mainwaring, P. Stewart, J. Marriott, Development and application of a micro-capillary rheometer for in-vitro evaluation of parenteral injectability, J. Pharm. Pharm. 56 (2004) 709–716.
[24] R.B. Bird, W.E. Stewart, E.N. Lightfoot, Transport Phenomena, Second edition, John Wiley & Sons, New York, 2007.
[25] R.A. Hingson, J.G. Hughes, Clinical studies with jet injection: a new method of drug administration, Curr. Res. Anesthesia Analgesia 26 (1947) 221–230.
[26] S. Mitragotri, Current status and future prospects of needle-free liquid jet injectors, Nat. Rev. Drug Discov. 5 (2006) 543–548.
[27] J. Schramm-Baxter, J. Katrencik, S. Mitragotri, Jet injection into polyacrylamide gels: investigation of jet injection mechanics, J. Biomech. 37 (2004) 1181–1188.
[28] R.F. Donnelly, D.I.J. Morrow, P.A. McCarron, M.J. Garland, A.D. Woolfson, Influence of solution viscosity and injection protocol on distribution patterns of jet injectors: application to photodynamic tumour targeting, J. Photochem. Photobiol. B 89 (2007) 98–109.
[29] A. Arora, M.R. Prausnitz, S. Mitragotri, Micro-scale devices for transdermal drug delivery, Int. J. Pharma. 364 (2008) 227–236.
[30] J.C. Stachowiak, T.H. Li, Arora Anubhav, S. Mitragotri, D.A. Fletcher, Dynamic control of needle-free jet injection, J. Control. Release 135 (2009) 104–112.
[31] J.C. Stachowiak, M.G. von Muhlen, T.H. Li, L. Jalilian, S.H. Parekh, D.A. Fletcher, Piezoelectric control of needle-free transdermal drug delivery, J. Control. Release 124 (2007) 88–97.
[32] T.M. Grant, K.D. Stockwell, J.B. Morrison, D.D. Mann, Effect of injection pressure and fluid volume and density on the jet dispersion pattern of needle-free injection devices, Biosyst. Eng. 138 (2015) 59–64.
[33] X. Li, B. Ruddy, A. Taberner, Characterization of needle-assisted jet injections, J. Control. Release 243 (2016) 195–203.
[34] A. Schoubben, A. Cavicchi, L. Barberini, A. Faraon, M. Berti, M. Ricci, P. Blasi, L. Postrioti, Dynamic behavior of a spring-powered micronozzle needle-free injector, Int. J. Pharm. 491 (2015) 91–98.
[35] O.A. Shergold, N.A. Fleck, T.S. King, The penetration of a soft solid by a liquid jet, with application to the administration of a needle-free injection, J. Biomech. 39 (2006) 2593–2602.
[36] N. Inoue, H. Todo, D. Iidaka, Y. Tokudome, F. Hashimoto, T. Kishino, K. Sugibayashi, Possibility and effectiveness of drug delivery to skin by needle-free injector, Int. J. Pharm. 391 (2010) 65–72.
[37] K. Benedek, E. Walker, L.A. Doshier, R. Stout, Studies on the use of needle-free injection device on proteins, J. Chromot. A 1079 (2005) 397–407.
[38] J. Seok, C.T. Oh, H.J. Kwon, T.R. Kwon, E.J. Choi, S.Y. Choi, S.K. Mun, S.-H. Han, B.J. Kim, M.N. Kim, Investigating skin penetration depth and shape following needle-free injection at different pressures: a cadaveric study, Lasers Surg. Med. 48 (2016) 624–628.
[39] J. Schramm, S. Mitragotri, Transdermal drug delivery by jet injectors: energetics of jet formation and penetration, Pharm. Res. 19 (2002) 1673–1679.
[40] J. Schramm-Baxter, S. Mitragotri, Needle-free jet injections: dependence of jet penetration and dispersion in the skin on jet power, J. Control. Rel. 97 (2004) 527–535.
[41] Y. Michinaka, S. Mitragotri, Delivery of polymeric particles into skin using needle-free liquid jet injectors, J. Control. Rel. 153 (2011) 249–254.
[42] J. Baxter, S. Mitragotri, Jet-induced skin puncture and its impact on needle-free jet injections: experimental studies and a predictive model, J. Control. Release 106 (2005) 361–373.
[43] A. Taberner, N.C. Hogan, I.W. Hunter, Needle-free injection using real-time controlled linear Lorentz-force actuators, Med. Eng. Phys. 34 (2012) 1228–1235.
[44] J.W. McKeage, B.P. Ruddy, P.M.F. Nielsen, A.J. Taberner, The effect of jet speed on large volume jet injection, J. Control. Release 280 (2018) 51–57.
[45] J.W. McKeage, B.P. Ruddy, P.M.F. Nielsen, A.J. Taberner, Power-efficient controlled jet injection using a compund ampoule, J. Control. Release 291 (2018) 127–134.
[46] L. Linn, B. Boyd, H. Ointchev, t. King, S.J. Farr, The effects of system parameters on *in vivo* injection performance of a needle-free injector in human volunteers, Pharm. Res. 24 (2007) 1501–1507.
[47] S. Hama, M. Arata, I. Nakamura, T. Kasetani, S. Itakura, H. Tsuchiya, T. Yoshiki, K. Kogure, Prevention of tumor growth by needle-free injection of anti-C7orf24 siRNA, Cancer Gene Ther. 19 (2012) 553–557.
[48] G.E. Theintz, P.C. Sizonenko, Risks of jet injection of insulin in children, Eur. J. Pediatr. 150 (1991) 554–556.
[49] U. Schneider, R. Birnbacher, E. Schober, Painfulness of needle and jet injection in children with diabetes mellitus, Eur. J. Pediatr. 153 (1994) 409–410.
[50] A. Arora, I. Hakim, Rathnasingham, R. Srinivasan, D.A. Fletcher, S. Mitragotri, Needle-free delivery of macromolecules across the skin by nanoliter-volume pulsed microjets, PNAS 104 (2007) 4255–4260.
[51] P. Delrot, S.P. Hauser, J. Krizek, C. Moser, Depth-controlled laser-induced jet injection for direct three-dimensional liquid delivery, Appl. Phys. A Mater. Sci. Process. 124 (615) (2018).
[52] Y. Tagawa, N. Oudalov, A. El Ghalbzouri, C. Sun, D. Lohse, Needle-free injection into skin and soft matter with highly focused microjets, Lab Chip 13 (2013) 1357.
[53] Kiyama, A., Endo, N., Kawamoto, S., Katsuta, C., Oida, k., Tanaka, A. & Tagawa, Y., Visualization of penetration of a high-speed focused microjet into gel and animal skin J. Vis. doi: https://doi.org/10.1007/s12650-019-00547-8.
[54] C. Berrospe-Rodriguez, C.W. Visser, S. Schlautmann, D.F. Rivas, R. Ramos-Garcia, Toward jet injection by continuous wave laser cavitation, J. Biomed. Optics 22 (2017) 105003.
[55] Miyazaki, H., Atobe, S., Suzuki, T., Iga, H. & Terai, K., Development of a pyro-drive jet injector with controllable jet pressure J. Pharm. Sci., doi: https://doi.org/10.1016/j.xphs.2019.02.021.
[56] S. Resik, A. Tejeda, O. Mach, C. Sein, N. Molodecky, C. Jarrahian, L. Saganic, D. Zehrung, M. Fonesca, M. Diaz, N. Alemany, G. Garcia, L.H. Hung, Y. Martinez, R.W. Sutter, Needle-free jet injector intradermal delivery of fractional dose inactivated poliovirus vaccine: association between injection quality and immunogenicity, Vaccine 33 (2015) 5873–5877.
[57] A.J. Mohammed, S. Al-Awaidy, S. Bawikar, et al., Fractional doses of inactivated poliovirus vaccine in Oman, N.E. J. Med. 365 (25) (2010) 2351–2359.
[58] D. Soonawala, P. Verdijk, A.J. Wijmenga-Monsuur, C.J. Boog, P. Koedam, L.G. Visser, N.Y. Rots, Intradermal fractional booster of inactivated poliomyelitis vaccine with a jet injector in healthy adults, Vaccine 31 (2013) 3688–3694.
[59] M.T. Yousafzai, A.F. Saleem, O. Mach, A. Baig, R.W. Sutter, A.K.M. Zaidi, Feasibility of conducting intradermal vaccination campaign with inactivated poliovirus using Tropis intradermal needlefree injection system, Karachi, Pakistan, Heliyon 3 (2017) e00395.
[60] A. Bavdekar, J. Oswal, P.V. Ramanan, et al., Immunogenicity and safety of measles-mumps-rubella vaccine delivered by disposable-syringe jet injector in India: a randomized, parallel group, non-inferiority trial, Vaccine 36 (2018) 1220–1226.
[61] J.K. Simon, C. Michaela, M.F. Pasetti, et al., Safety, tolerability, and immunogenicity of inactivated trivalent seasonal influenza vaccine administered with a needle-free disposable syringe jet injector, Vaccine 29 (2011) 9544–9550.
[62] K.E. Broderick, A.S. Khan, N.Y. Sardesai, DNA vaccination in skin enhanced by electroporation, Methods Mol. Biol. 1143 (2014) 123–130.
[63] J.B. McCoy, J.M. Mendoza, K.W. Spik, C. Badger, A. Gomez, C.S. Schmaljohn, N.Y. Sardesai, K.E. Broderick, A multi-head intradermal electroporation device allows for tailored and increased dose DNA vaccine delivery to the skin, Hum. Vaccine Immunother. 3 (2014) 10.
[64] K.E. Broderick, L.M. Humeau, Electroporation-enhanced delivery of nucleic acid vaccines, Expert Rev. Vaccines 14 (2015) 195–204.
[65] M.R. Prausnitz, A practical assessment of transdermal drug delivery by skin electroporation, Adv. Drug Deliv. Rev. 35 (1999) 61–76.
[66] F. Cilurzo, F. Selmin, P. Minghetti, M. Adami, E. Bertoni, S. Lauria, L. Montanari, Injectability evaluation: an open issue, Pharm. Sci. Tech. 12 (2011) 604–608.
[67] S.P. Lin, R.D. Reitz, Drop and spray formation from a liquid jet, Annu. Rev. Fluid Mech. 30 (1998) 85–105.
[68] M.J. McCarthy, N.A. Molloy, Review of stability of liquid jets and the influence of nozzle design, Chem. Eng. J. 7 (1) (1974) 1.
[69] C.J. Howland, A. Antkowiak, J.R. CastrejÃ³n-Pita, S.D. Howison, J.M. Oliver, R.W. Style, A.A. CastrejÃ³n-Pita, It's harder to splash on soft solids, Phys. Rev. Lett. 117 (184502) (2016).
[70] J.C.J. Wei, G.A. Edwards, D.J. Martin, H. Huang, M.L. Crichton, M.A.F. Kendall, Allometric scaling of skin thickness, elasticity, viscoelasticity to mass for micro-medical device translation: from mice, rats, rabbits, pigs to humans, Nat. Sci. Rep. 7 (15885) (2017).
[71] C. Flynn, A. Taberner, P. Nielsen, Measurement of the force-displacement response of in-vivo human skin under a rich set of deformations, Med. Eng. Phys. 33 (2011) 610–619.